

Detecting buried non-metal objects using soil magnetic susceptibility measurements

Haoping Huang, I. J. Won and Bill San Filippo
Geophex, Ltd, 605 Mercury Street, Raleigh, NC, USA 27603-2343

ABSTRACT

Soil magnetic susceptibility is always greater than zero and is detectable using an electromagnetic (EM) induction sensor. When the frequency-domain EM response is affected by magnetic polarization, the in-phase component becomes negative at the low frequency and proportional to the ground magnetic susceptibility. The in-phase measurement can thus be used to compute the apparent magnetic susceptibility. This approach provides a means of detecting a buried object based on its susceptibility contrast to the host medium. For example, an M19 anti-tank mine is physically large (33cm×33cm×9cm) but has so little metal that metal detectors can miss it. When an M19 is buried in soil, it produces a cavity in magnetic susceptibility, which may be detected as a region of low or anomalous apparent susceptibility compared to the surrounding area. We derived a simple formula to compute the apparent magnetic susceptibility from the in-phase data at the resistive limit. The behavior of the apparent susceptibility for layered earth models has been studied using synthetic data. Apparent susceptibility anomalies may be predicted from these studies based on the susceptibility contrast, and geometry of the sensor and target. Finally, we present experimental data obtained using two sensors, a GEM-2 and a GEM-3.

Keywords: Electromagnetic Induction, Resistive Limit, Magnetic susceptibility, Nonmetal object Detection

1. INTRODUCTION

New broadband electromagnetic (EM) sensors, for example the GEM family, have been used to detect and identify unexploded ordnance (UXO), landmines and many other objects (Won et al., 1997, 1998; Keiswetter et al., 1997; Gao et al., 2000; Norton and Won, 2001; Norton et al., 2001a and 2001b; Huang and Won, 2001, 2003a and 2003b). In such applications, we measure the electromagnetic induction spectroscopy (EMIS), and match the spectrum against signatures from known objects that are stored in a library. A key to success in identifying an object is to extract the spectrum produced only by the target. This requires removing the EM response of the background geology, which affects largely the in-phase component of the secondary magnetic field due to magnetic soil or rock (Huang and Fraser, 1998, 2000; Huang and Won, 2000). On one hand, the response over magnetic geology is noise in detecting and identifying a metal object. On the other hand, it is a useful signal in detecting a non-metal object, such as a large plastic antitank mine. Since soil magnetic susceptibility is always greater than zero, a buried large plastic object produces a cavity in magnetic susceptibility, which may be detected as a region of low or anomalous apparent susceptibility compared to the surrounding area.

Non-metal objects may be detected by radio imaging or ground penetrating radar (GPR) based on the ground dielectric contrast. Such technologies for landmine detection are still under development. Alternately, the commercially available EM sensors (e.g., GEM-3) may be used to detect large non-metal landmines based on the magnetic susceptibility contrast. Since the in-phase component of the secondary magnetic field depends only upon the ground susceptibility and the sensor geometry at the low induction number, it is easy to convert to the apparent susceptibility that yields a higher resolution to near-surface magnetic features.

In this paper, we study the feasibility to detect large non-metal objects, such as an M19 antitank mine, based on the apparent magnetic susceptibility contrast measured with an EM sensor (e.g., GEM family). We present the results from the theoretical modeling and experiments.

2. APPARENT SUSCEPTIBILITY AT RESISTIVE-LIMIT

The basic model used is depicted in Figure 1 where two electromagnetic sensors are at a height, h , over a magnetic permeable half-space. The transmitter and receiver, either separated by a distance, s , or concentric, are small horizontal coils. The secondary magnetic field H_s , normalized by the primary field H_0 at the receiving coil, has been described by many authors (e.g., Ward and Hohmann, 1988). Here, we write it as

$$\frac{H_s}{H_0} = L^{n+1} \int_0^\infty \frac{u_1 - \lambda}{u_1 + \lambda} \lambda^n e^{-2\lambda h} J_k(\lambda L) d\lambda, \quad u_1 = \frac{\sqrt{\lambda^2 + i\omega\sigma\mu}}{\mu_r}. \quad (1)$$

where J_k is the Bessel function of the first kind of order k , $n=2$ and $k=0$ for horizontal coplanar coil pairs (e. g., GEM-2 flat orientation), $n=1$ and $k=1$ for vertical coplanar (e. g., GEM-2 oriented on edge) and horizontal concentric (e. g., GEM-3) coil pairs. Here, ω is the angular frequency, σ is the conductivity, μ is the magnetic permeability, and μ_r is the relative magnetic permeability. L stands for either the coil separation s , or the radius of transmitter coil r for concentric coil pairs.

The complex quantity H_s/H_0 when multiplied by 10^6 is in units of parts per million (ppm) and consists of the real (in-phase I) and imaginary (quadrature Q) components. Figure 2 shows the in-phase and quadrature components as a function of induction number $\theta=(\omega\sigma\mu/2)^{1/2}L$ for various values of magnetic susceptibility $\kappa = \mu_r - 1$ over a homogeneous half-space. The resistive-limit zone is depicted as below the dashed lines, where the EM response becomes dominated by the magnetization effect, which is in-phase with, and in the same direction as, the primary field, and is frequency-independent. The quadrature component, however, is insensitive to the magnetic susceptibility. This feature can be used to convert the EM data to the apparent conductivity using quadrature components at two frequencies without influence of susceptibility in magnetic environments (Huang and Fraser, 2002). The resistive-limit range varies with the susceptibility; for example, it would be $\theta < 0.025$ for $\kappa < 0.0001$, and $\theta < 2$ for $\kappa < 1$ for horizontal coplanar coil pairs. For small handheld sensors, such as GEM-2 and GEM-3, the resistive-limit solution covers, when a low frequency is used, all natural geology.

At the resistive-limit, $\omega\sigma \rightarrow 0$, Equation (1) can be integrated, and simplified as

$$I = \frac{-\kappa}{2 + \kappa} G, \quad (2)$$

where G is a geometry factor, and can be written as

$$G = \frac{8 \left(\frac{h}{s} \right)^2 - 1}{\left[4 \left(\frac{h}{s} \right)^2 + 1 \right]^{5/2}}, \quad \text{for horizontal coplanar coil pairs, and} \quad (3)$$

$$G = \frac{1}{\left[4 \left(\frac{h}{L} \right)^2 + 1 \right]^{3/2}}, \quad \text{for vertical coplanar and horizontal concentric coil pairs.} \quad (4)$$

In Equation (4), L stands for the coil separation s for vertical coplanar coil-pairs, and for the radius r of transmitter coil for horizontal concentric coil pairs. The in-phase response I depends upon the magnetic susceptibility and the ratio of sensor height to the sensor size. From Equation (2), we have

$$\kappa = \frac{-2I}{I + G}. \quad (5)$$

If the earth were homogeneous within the volume affected by the primary magnetic field, the magnetic susceptibility κ obtained from Equation (5) would be the true susceptibility; otherwise it would be the apparent susceptibility κ_a .

3. APPARENT SUSCEPTIBILITY ANOMALY OF A LAYERED MODEL

We will first show how the apparent susceptibility behaves over a layered earth model. A two-layer model may be used to simulate the situation of a buried object so large compared with the size of EM sensor that all dimensions can be ignored; while a three-layer model can be used for an object with a vertical dimension much less than its horizontal dimensions.

Figure 3 shows the apparent susceptibility curves as a function of L/t_1 , the ratio of sensor size to upper-layer thickness t_1 for the two-layer model with the magnetic susceptibility contrast κ_2/κ_1 from 1/100 to 100. When L/t_1 is small, the upper layer (soil) is very thick compared with the sensor size. In this case, the lower layer, i.e., the buried object, makes no contribution to the in-phase response, so that the apparent susceptibility is equal to the true susceptibility of the upper layer. As L/t_1 increases (i.e., the upper layer becomes thinner compared with the sensor size), the apparent susceptibility approaches the susceptibility of the lower layer.

The detection of the lower layer depends upon the ratio of sensor size to thickness of the upper layer and the susceptibility contrast between the two layers. If 15% deviation from $\kappa_a/\kappa_1=1$ is considered as a significant anomaly, we can estimate maximum depth of the lower layer that can be detected. For instance, when $\kappa_2/\kappa_1 \leq 0.2$, a sensor with a coil separation of 1.66 m can detect a lower layer at depth of 1.84 m ($s/t_1=0.9$), while a concentric sensor with a radius of 0.2 m can detect a lower layer at depth of 0.14 m ($r/t_1=1.4$). The detectability of the lower layer will increase for a more permeable lower layer ($\kappa_2/\kappa_1 > 1$).

The apparent susceptibility for a three-layer model is shown in Figure 4 as functions of the ratio of the sensor size L to thickness of the upper layer t_1 and the ratio of thickness of the middle layer t_2 to that of the upper layer t_1 , for susceptibility contrasts of $\kappa_2/\kappa_1=0.01$ and 100. The dashed contour line is the 15% anomaly threshold for detecting the middle layer, which is supposed to be detected when $\kappa_a/\kappa_1 < 0.85$ for $\kappa_2/\kappa_1 < 1$ and $\kappa_a/\kappa_1 > 1.15$ for $\kappa_2/\kappa_1 > 1$. Figure 4 may be used to estimate whether a specific target can be detected for a given sensor and height. For instance, antitank mine M19 has a size of 33cm×33cm×9cm, and it is usually buried at a depth of 7 cm. A buried M19 may be treated as a three-layer model when a concentric sensor, such as the GEM-3, is used. This is because the effects of lateral inhomogeneities are largely reduced by measuring only the vertical component of the magnetic field at the center of the transmitter coil. If a sensor with transmitter radius of 20 cm is used, then we have $t_2/t_1=9\text{cm}/7\text{cm}=1.29$ and $r/t_1=20\text{cm}/7\text{cm}=2.86$. In this case, we may obtain an anomaly of $\kappa_a/\kappa_1=0.76$ for a sensor height of 12.5cm ($h/r=0.625$). This means that the middle layer (M19) may produce an apparent susceptibility anomaly of 24% ($|\kappa_a/\kappa_1-1| \times 100$). If we sweep the sensor as close as possible to the surface, an anomaly of 35% ($\kappa_a/\kappa_1=0.65$) may be observed as shown in Figure 4e. Also, if magnetic susceptibility is higher for a buried non-metal object than for soil, the object will be detected easily as shown in Figures 4b and 4d.

The apparent susceptibility of a finite object may be modeled by physical modeling. Figure 5 shows such an example, where a non-metal box sized 32cm×32cm×13cm was buried in soil at depth of 13cm. The EM data were collected at

2490 Hz along a profile over the box, and the in-phase data were converted into the apparent susceptibility. As the sensor approaches the target, the apparent susceptibility decreases rapidly, and reaches minimum around the edge of the target, then, it slightly rises over the center of the object. The peak occurring around the edge is known as the edge effect. If the target was so large compared with the sensor that it could be considered infinite in horizontal extent, the apparent susceptibility would rise sharply to the layered earth value over the target.

4. EXPERIMENTAL RESULTS

We performed experiments using both GEM-2 and GEM3 broadband EM sensors.. The former may be used to detect relatively large targets, such as caves, sewers, and underground facilities, while the later is better suited to detect small objects, such as non-metal antitank mines. Two examples will be shown below, one from the Geophex test site in Raleigh, North Carolina and the other from a US army test site.

Figure 6 is the susceptibility map of the Geophex test site, which was derived from GEM-2 in-phase data at 5,430 Hz. The host soil is dense red clay known as Piedmont Clay, of which resistivity is about 90 ohm-m and magnetic susceptibility from 0.0001 to 0.0015. The major feature is the linear susceptibility low in the middle and north of the map, which corresponds to the known storm sewer below the surface.

The second example is from a US army test site which consists of a small “calibration plot” containing identified landmines and clutter objects, and a large blind test area that contains 980 blind one meter test squares. Each square may contain at the center a mine, clutter, or nothing. We performed a demonstration survey using the GEM-3, with a 20 cm-radius sensor, at 10 frequencies ranging from 750 Hz to 23,970 Hz. The purpose of the survey was to identify landmines that contain metal parts (Huang and Won, 2003b). However, we also tested the idea described above. Figure 7 shows anomalies of the apparent magnetic susceptibility for three squares (D6, D8, and E21) in the calibration plot. Squares D6 and D8 contain M19 at depths of 1.25 inch (3.175 cm) and 2.5 inch (6.35 cm), while square E21 contains an irregular stone at a depth of 2 inch (5.08 cm). The landmines produce anomaly amplitudes of 50% and 42%, which are easy to be recognized, while the stone produces no anomaly. Figure 8 shows the susceptibility profiles from squares D2 and L6 in the blind test grid, where M19s were buried at depths of 2.63 inch (6.68 cm) and 1.5 inch (3.81cm), respectively. We can definitely see the susceptibility lows caused by the magnetic cavity.

5. CONCLUSIONS

Soil magnetic susceptibility is always greater than zero and is detectable using an EM induction sensor at the resistive limit. Unlike a magnetometer that measures the Earth’s static magnetic field, an EM sensor illuminates and provides information about near-surface magnetic features. A buried non-metal object such as a large plastic landmine may produce a cavity in magnetic susceptibility, which may be detected as a region of low or anomalous apparent susceptibility compared to the surrounding area.

A simple formula has been derived to compute the apparent magnetic susceptibility from the in-phase data at the resistive limit. The behavior of the apparent susceptibility for layered models has been studied using. Apparent susceptibility anomalies may be predicted from these studies based on the susceptibility contrast, and geometry of the sensor and target. Experimental examples show that the storm sewer and antitank mine, M19, can be detected from the apparent susceptibility contrast.

REFERENCES

1. Gao, P., Collins, L., Garber, P. M., Geng, N. and Carin, L., “Classification of landmine-like metal targets using wideband electromagnetic induction”, *IEEE Transactions on Geoscience and Remote Sensing*, **38**, no. 3, 1352-1361, 2000.
2. Huang, H. and Fraser, D. C., “Magnetic permeability and electrical conductivity mapping with a multifrequency airborne EM system”, *Exploration Geophysics*, **29**, 249-253, 1998.

3. Huang, H., and Fraser, D.C., "Airborne resistivity and susceptibility mapping in magnetically polarizable areas", *Geophysics*, **65**, 502-511, 2000.
4. Huang, H., and Fraser, D. C., "The use of quad-quad resistivity in helicopter electromagnetic mapping", *Geophysics*, **67**, 459-467, 2002.
5. Huang, H., and Won, I. J., "Conductivity and susceptibility mapping using broadband electromagnetic sensors", *Journal of Environmental and Engineering Geophysics*, **5**, No.4, 31-41, 2000.
6. Huang, H., and Won, I. J., "Characterization of UXO-like targets using broadband electromagnetic induction sensors", Accepted for publication in *IEEE Transactions on Geoscience and Remote Sensing*, 2003a.
7. Huang, H., and Won, I. J., "Automated identification of landmines using normalized electromagnetic induction spectroscopy", Accepted for publication in *IEEE Transactions on Geoscience and Remote Sensing*, 2003b.
8. Keiswetter, D., Novikova, E., Won, I.J., Hall, T., and Hanson, D., "Development of a monostatic, multifrequency electromagnetic mine detector", *Society of Optical Engineering*, **3079**, 831-839, 1997.
9. Norton, S. J. and Won, I. J., "Identification of Buried Unexploded Ordnance from Broadband Electromagnetic Induction Data", *IEEE Transactions on Geoscience and Remote Sensing*, **39**, 2253-2261, 2001.
10. Norton, S. J. and Won, I. J., and Cespedes, E. R., "Ordnance/Clutter Discrimination Based on Target Eigenvalue Analysis", *Subsurface Sensing Tech. Appl.*, **2**, 285-298, 2001a.
11. Norton, S. J., Won, I. J., and Cespedes, E. R., "Spectral identification of buried unexploded ordnance from low-frequency electromagnetic data", *Subsurface Sensing Tech. Appl.*, **2**, 177-189, 2001b.
12. Ward, S. H., and Hohmann, G. W., *Electromagnetic Methods in Applied Geophysics*, Theory, 130-311, Society of Exploration Geophysicists, 1988.
13. Won, I. J., Keiswetter, D., Hanson, D., Novikova, E., and Hall, T., "GEM-3: A monostatic broadband electromagnetic induction sensor", *Journal of Environmental and Engineering Geophysics*, **2**, No. 1, 53-64, 1997.
14. Won, I. J., Keiswetter, D., and Novikova, E., "Electromagnetic induction spectroscopy", *Journal of Environmental and Engineering Geophysics*, **3**, No. 1, 27-40, 1998.

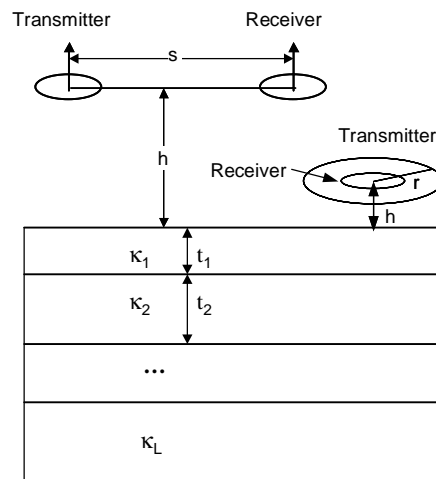


Figure 1: The half-space model with an EM sensor at height h . The conductivities of each layer can be ignored in the resistive (low-frequency) limit.

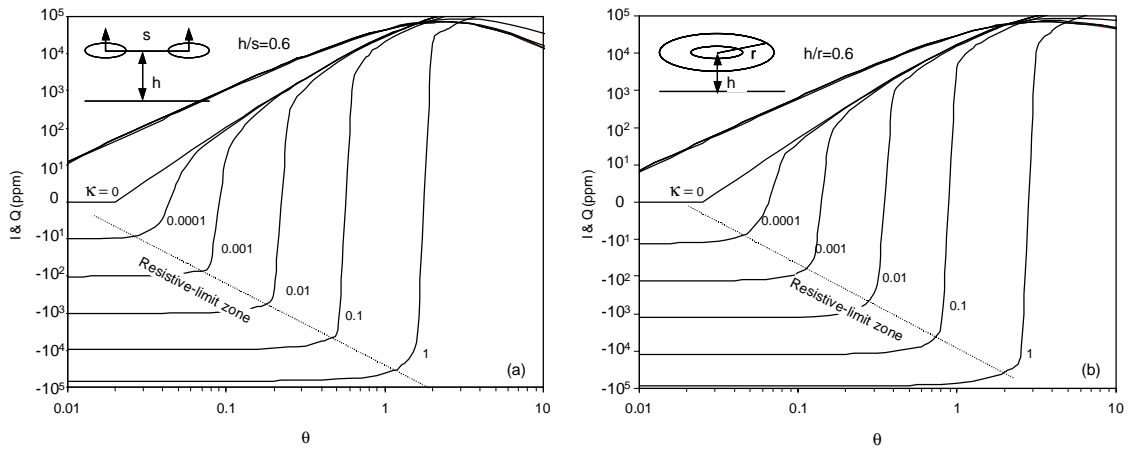


Figure 2: In-phase I and quadrature Q components of the response of a homogeneous half-space plotted as a function of induction number θ for various values of the magnetic susceptibility κ , for both separated (a) and concentric (b) coil configurations.

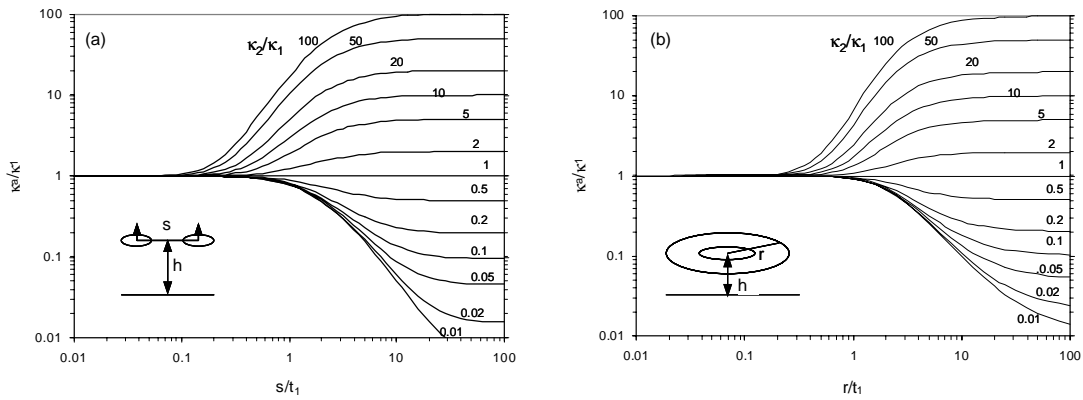


Figure 3: The apparent susceptibility curves for a suite of two-layer models for the permeability ratios κ_2/κ_1 from 0.01 to 100, for both coplanar (a) and concentric (b) coil configurations.

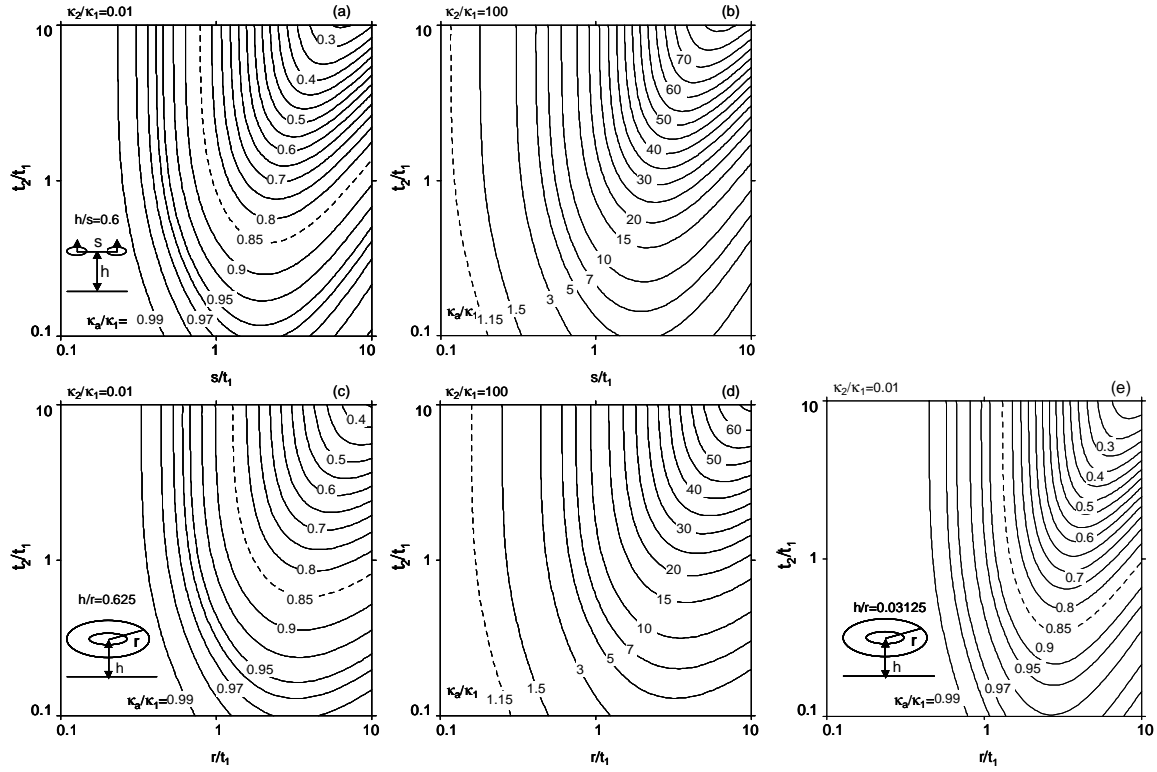


Figure 4: The apparent susceptibility contours for a suite of three -layer models with fixed susceptibility contrasts κ_2/κ_1 of 0.01 and 100. Panels (a) and (b) for coplanar coil pairs, and (c) and (d) for concentric coil pairs. Panel (e) is for concentric coil pairs with $h/r=0.031$.

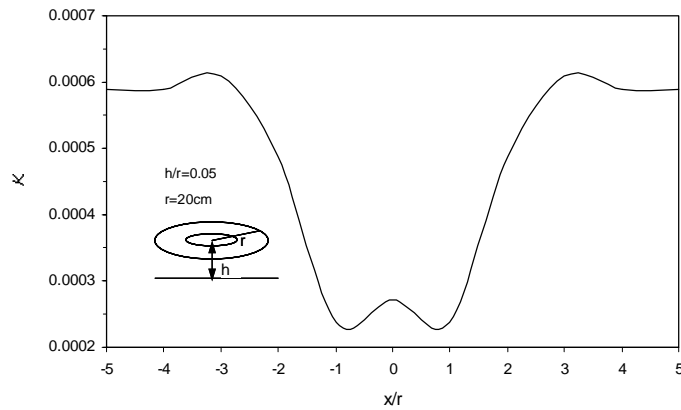


Figure 5: The apparent susceptibility of a non-metal box sized 32cm×32cm×13cm that was buried in soil at depth of 13cm. The horizontal axis is distance, x normalized by the radius of transmitter coil, r . The origin is over the center of the box.

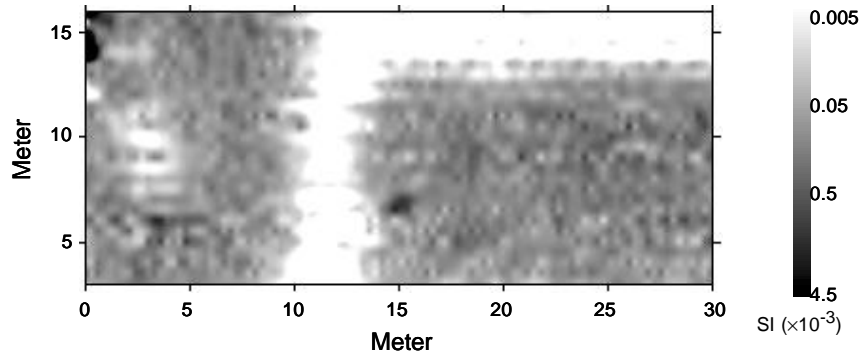


Figure 6: The apparent susceptibility map of the test site in Raleigh, North Carolina.

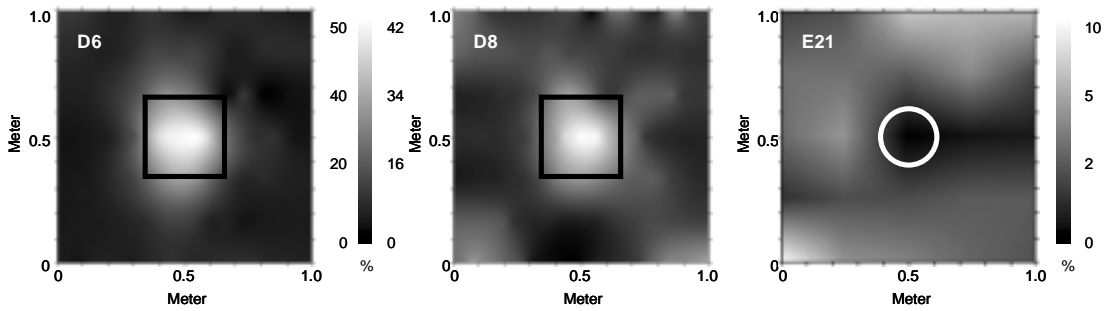


Figure 7: The apparent susceptibility images at three 1m×1m squares, where antitank mines M19 were buried in D6 and D8, and a stone in E21. The squares and circle present the size of the targets.

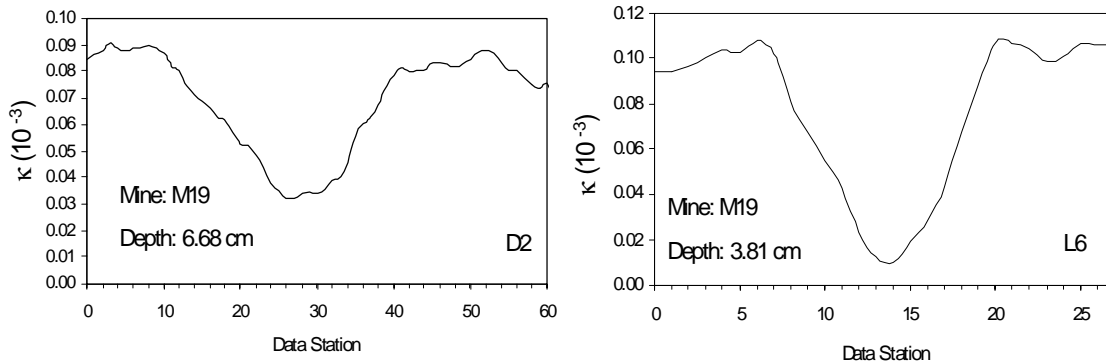


Figure 8: The apparent susceptibility anomalies observed at D2 and L6 in the blind test grids, where M19s were buried at depths of 6.68 cm and 3.81 cm. The length of profile is 1.4 m.